arXiv:1511.01713v1 [cond-mat.quant-gas] 5 Nov 2015

Topological superfluids with time-reversal symmetry from s-wave interaction in a bilayer system

Beibing Huang*,[1,2] Pak Hong Chui*,[1] Jia Liu,[1] Chuanwei Zhang,[3] and Ming Gong[1]

[1]*Department of Physics and Center for quantum Coherence, The Chinese University of Hong Kong Shatin, N.T., Hong Kong, China*
[2]*Department of Physics, Yancheng Institute of Technology, Yancheng, 224051, P. R. China*
[3]*Department of Physics, The University of Texas at Dallas, Richardson, TX 75080, USA*

(Dated: November 6, 2015)

Topological superconducting phases with time-reversal (TR) symmetry have been widely explored in recent years. However the involved unconventional pairings are generally implausible in realistic materials. Here we demonstrate via detailed self-consistent calculation that these topological phases with TR symmetry in DIII and BDI classes can be realized in a spin-orbit coupled bilayer system with only s-wave interaction. The bilayer freedom enables the definition of TR symmetry between the layers even in the presence of local Zeeman fields, which we propose to be realized using four laser beams. The gapped phase in DIII class is characterized by $\mathbb{Z}_2$, while all the gapless phases in these two classes are characterized by nontrivial winding numbers and are also manifested from the Majorana flat bands. We also unveil the intimate relation between TR symmetry and mirror symmetry due to phase locking effect between the two layers, which harbors the mirror symmetry protected topological phases. We finally demonstrate that these phases will not be spoiled by interlayer pairings.

There is a major effort in realizing unpaired Majorana fermions (MFs) in both condensed matter physics and cold atom physics, which have important applications in topological quantum computations[1]. These systems include p-wave superconducting phases in Sr_2RuO_4[2, 3], Helium-3[4] and fully spin polarized ultracold atoms[5, 6], and the $\nu = 5/2$ fractional quantum Hall state[1, 7]. Unfortunately, whether these systems can be used to realize the elusive MFs is still a controversial issue due to the lacking of convincing evidences. The conceptional breakthrough in recent years is based on the idea that these exotic quantum phases can be realized using the conventional s-wave interaction, spin-orbit coupling (SOC) and Zeeman field[8–11]. Very recently some pioneering experiments both in one-dimensional (1D) nanowires and iron chain on the realization of MFs has been carried out[12–16]. Remarkably, the localized wave functions at the two ends with zero eigenenergy have been identified[16], which provide important evidence for the realization of MFs. These systems belong to topological D class from the Cartan classification due to absence of time-reversal (TR) symmetry[17, 18]. In all these systems *only* the topological protected gapped phase can be realized, while the topological phase transition is characterized either by the Chern number of the occupied bands, or somewhat equivalently the Pfaffian (Pf) of the Hamiltonian at the particle-hole (PH) invariant point(s)[19].

These progress strongly stimulates the persuit of topological superconducting phases with TR symmetry. However, these fantastical phases generally involve some *unconventional* $p_x + ip_y$[20], $d_{x^2-y^2}$[21–25] and $s_\pm$[26–28] pairings, which are implausible in realistic materials. Therefore we have the intriguing question that whether there phases can exist with only s-wave interaction? Here, instead of seeking for other new materials, we explore these phases in a synthetic bilayer system where the bilayer freedom enables the definition of nonlocal TR symmetry between the layers. While the single layer physics is well-known in some sense, we show that the interlayer tunnelings and TR symmetry can lead to fundamentally different superconducting phases. We explore the topological protected gapped and gapless phases in both DIII and BDI classes in this platform, in which the fully gapped phase in DIII phase is characterized by $\mathbb{Z}_2$, while all the gapless phases are characterized by nontrivial winding numbers [29, 30] around the topological defects — the Dirac cones — in momentum space and are also manifested from the Majorana flat bands (MFBs)[31]. We have proposed a scheme to realize some of these phases in experiments. These results are confirmed using detailed self-consistent calculation, in which the order parameters and chemical potential are determined by the extrema of the free energy. We also unveil the intimate relation between TR and mirror symmetries in our models due

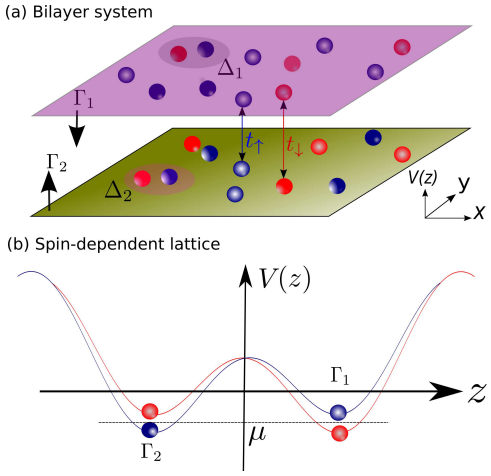

FIG. 1. **Bilayer system for TR invariant superfluids**. (b) The bilayer structure can be realized by imposing a strong double-well potential along the z direction. The possibility of individual tunability of the local Zeeman fields, spin-dependent tunnelings and the SOC coefficients can be used to realize different topological models with TR symmetry. (b) Realization of local Zeeman fields with opposite sign in the bilayer system for T_{xy} model via a spin-dependent lattice; see more details in Methods.

to phase locking effect between the pairings in the two layers, from which we realize some mirror symmetry protected gapped and gapless phases. We finally demonstrate that these phases will not be spoiled by the interlayer pairings. We expect these new phases to greatly enrich our understanding of topological superconducting phases and related transitions.

Results

Physical Model. We first briefly discuss the topological superfluids in a single layer system, which has been intensively studied in recent years[32–36]. In this model the Zeeman field is used to break the Kramers degeneracy at zero momentum, so that the chemical potential can fill just one band, around which an effective p-wave pairing can be induced. We found that the topological phase can be realized in a narrow parameter regime even at finite temperature though the Zeeman field is (much) larger than the pairing strength[32, 33], so the induced p-wave pairing provides a new mechanism to go beyond the Chandrasekhar-Clogston limit[43, 44]. The recent interests in this system also include the topological inhomogeneous superfluids[37–39], the quench dynamics of the topological superfluids[40, 41] and the topological superradiant state[42]. Thus the exploring of these exotic phases in this model is still an important topic in modern research.

To explore an experimental realization of the topological phases with TR symmetry, we consider a two-dimensional (2D) bilayer system, see the schematic structure in Fig. 1, which can be realized by imposing a strong double-well potential along the z direction[45, 46]. This synthetic structure has been widely used in recent literatures for realizing some exotic phases in solid systems[47, 48]. We first consider the case that both layers have identical SOC coefficients, $V_{\rm so}^i = (s_i k_y \sigma_x - \lambda_i k_x \sigma_y)$, where $\lambda_i = \alpha'$ and $s_i = \alpha$, $i = 1, 2$, are the SOC strength and σ_α are the Pauli matrices, and identical spin-dependent tunnelings $t_{\uparrow,\downarrow} = t$, but with different Zeeman fields Γ_i. The SOC in ultracold atoms both for fermions and bosons has been extensively explored using two coupled Raman beams[49–54], and very recently, the required 2D SOC has been realized in ^{40}K[55]. The barrier width between the two layers can be controlled by the laser intensity in experiments thus we can safely assume that only the intralayer pairings, which can be defined as $\Delta_i = \sum_{\mathbf{k}} g\langle c_{i\mathbf{k}\uparrow} c_{i-\mathbf{k}\downarrow}\rangle$, are important. Here g is the effective 2D interaction strength, $c_{i\mathbf{k}s}$ is the annihilate operator for particle with momentum $\mathbf{k}$ and spin s. The corresponding Bogoliubov-de Gennes (BdG) equation can be written as

$$\mathcal{H} = \begin{pmatrix} \mathcal{H}_0(\mathbf{k}) & \bar{\Delta} \\ \bar{\Delta}^\dagger & -\mathcal{H}_0^*(-\mathbf{k}) \end{pmatrix}, \tag{1}$$

with $\mathcal{H}_0(\mathbf{k})$ being the single particle Hamiltonian

$$\mathcal{H}_0(\mathbf{k}) = \begin{pmatrix} \epsilon_{\mathbf{k}} + \Gamma_1 & \rho_{1\mathbf{k}} & -t_\uparrow & 0 \\ \rho_{1\mathbf{k}}^* & \epsilon_{\mathbf{k}} - \Gamma_1 & 0 & -t_\downarrow \\ -t_\uparrow & 0 & \epsilon_{\mathbf{k}} + \Gamma_2 & \rho_{2\mathbf{k}} \\ 0 & -t_\downarrow & \rho_{2\mathbf{k}}^* & \epsilon_{\mathbf{k}} - \Gamma_2 \end{pmatrix}. \tag{2}$$

Here $\epsilon_{\mathbf{k}} = \mathbf{k}^2/2m - \mu$, and $\rho_{i\mathbf{k}} = s_i k_y + i\lambda_i k_x$, and the concrete form of $\bar{\Delta}$ can be found in Methods (Eq. 31). We construct the BdG Hamiltonian in the Nambu spinor, $\Psi = (c_{1\mathbf{k}\uparrow}, c_{1\mathbf{k}\downarrow}, c_{2\mathbf{k}\uparrow}, c_{2\mathbf{k}\downarrow}, c_{1-\mathbf{k}\uparrow}^\dagger, c_{1-\mathbf{k}\downarrow}^\dagger, c_{2-\mathbf{k}\uparrow}^\dagger, c_{2-\mathbf{k}\downarrow}^\dagger)^T$. Notice that in ultracold atoms the order parameters and chemical potential should be solved self-consistently.

We define the TR operator $\mathcal{T}$ for the single particle Hamiltonian $\mathcal{H}_0$ in Eq. 2 and $\mathbb{T}$ for the BdG equation in Eq. 1, while both $\mathcal{T}^2 = -1$ and $\mathbb{T}^2 = -1$ are required for the topological superfluids in DIII class. The realization of topological BDI class superfluids with $\mathcal{T}^2 = +1$ and $\mathbb{T}^2 = +1$ will be discussed later. Obviously, without the Zeeman fields, this model has a nonlocal TR operator $\mathcal{T} = \rho_x \otimes \sigma_y K$, where ρ_α are Pauli matrices acting on the layer space and K is the complex conjugate operator. In this TR operator, the spin up (down) in one layer with momentum $\mathbf{k}$ is mapped to spin down (up) in the other layer with opposite momentum. This symmetry is still respected by the Zeeman fields when $\Gamma_1 = -\Gamma_2 = \Gamma$, which is the basic reason for the local Zeeman fields discussed before. These local Zeeman fields may be challenging to be realized in solid state system, however, in ultracold atoms — in the ideal condition — it can be realized using the following spin-dependent optical lattice,

$$V(z) = V_{\rm e}(z) + V_{\rm o}(z)\sigma_z, \tag{3}$$

where the subscripts e and o represent an even and odd function of z, respectively. The first term describes the spin-independent symmetric double-well potential, which has been realized in experiments[45, 46], and the second term means that the two layers have *exactly* opposite Zeeman fields. Such a structure can be realized using four counterpropagating laser beams (see details in Methods). An optical lattice that slightly deviates from the above scenario can still be used to realize the model with TR symmetry by fine-tuning the parameters.

The TR symmetry for the BdG equation is defined as $\mathbb{T} = \mathrm{diag}(\mathcal{T}, e^{i\phi}\mathcal{T})$, where ϕ is an arbitrary phase. The TR symmetry requires that $\mathcal{T}\bar{\Delta}\mathcal{T}^{-1}e^{-i\phi} = \bar{\Delta}$, namely, $\Delta_1 = \Delta_2^* e^{-i\phi}$. The phase ϕ is used to compensate the global phase of the order parameters such that only the relative phase between the two order parameters $\Delta_{1,2}$ is important. After self-consistent calculation (see details in Methods) we find that the two order parameters can be treated as real numbers simultaneously. More precisely, we find that the two layers can have zero relative phase and $\Delta_1/\Delta_2 > 0$ when the two tunnelings have the same sign; otherwise, the relative phase is $\pi/2$ and $\Delta_1/\Delta_2 < 0$. This effect is rather robust, and this feature is independent of other parameters such as binding energy, Zeeman fields *etc*. We further find that the relative phase between the two order parameters can only be introduced to the Hamiltonian by the complex tunneling terms. Hereafter, this effect is called the phase locking effect. For these reasons, throughout this work, we treat the two order parameters as real numbers in the numerical simulation. For this particular model we have

$$\mathbb{T} = \Lambda K = \tau_0 \otimes \mathcal{T}, \tag{4}$$

where τ_0 is a Paul matrix acting on PH space. The intrinsic PH operator is defined as $\mathbb{C} = \tau_x K$, which ensures that $\mathbb{C}\mathcal{H}(\mathbf{k})\mathbb{C}^{-1} = -\mathcal{H}(-\mathbf{k})$.

Hereafter, this model is dubbed as T_{xy} model to distinct itself from the other models studied in the following.

The Λ operator in Eq. 4 is essentially the mirror symmetry operator since in our model only the k_x component contains the imaginary number, which can change sign upon complex conjugation K. Thus we can define the mirror symmetry operator as $\mathcal{M}_y = \Lambda$, where

$$\mathcal{M}_y \mathcal{H}(k_x, k_y) \mathcal{M}_y^{-1} = \mathcal{H}(k_x, -k_y). \tag{5}$$

We can also define another mirror operator about k_y-axis as $\mathcal{M}_x = \mathbb{I} \cdot \mathcal{M}_y$, where $\mathbb{I} = \tau_z \otimes \rho_0 \otimes \sigma_z$ is the inversion symmetry operator, $\mathbb{I}\mathcal{H}(\mathbf{k})\mathbb{I}^{-1} = \mathcal{H}(-\mathbf{k})$. In this case,

$$\mathcal{M}_x \mathcal{H}(k_x, k_y) \mathcal{M}_x^{-1} = \mathcal{H}(-k_x, k_y). \tag{6}$$

Notice that both $\mathcal{M}_x$ and $\mathcal{M}_y$ are unitary hermitian operators and their eigenvalues are either -1 or $+1$ since $\mathcal{M}_{x,y}^2 = 1$.

These new symmetries can fundamentally change the topological invariant of the Hamiltonian in the mirror symmetric invariant 1D subspaces along k_x and k_y axes. To this end, we can diagonalize the mirror symmetry operators via a unitary transformation $U_\alpha \mathcal{M}_\alpha U_\alpha^{-1} = (\mathbf{I_4}, -\mathbf{I_4})$, where $\mathbf{I_4}$ is a 4×4 unity matrix and $\alpha = x, y$. Under this transformation we have

$$U_\alpha \mathcal{H}_\alpha U_\alpha^{-1} = \mathrm{diag}(M_1^\alpha, M_2^\alpha), \tag{7}$$

where $\mathcal{H}_x = \mathcal{H}(0, k_y)$ and $\mathcal{H}_y = \mathcal{H}(k_x, 0)$. In general $M_{1,2}^{x,y}$ can have totally different symmetries than the original Hamiltonian $\mathcal{H}$. The concrete form of these matrices and their topological invariants can be found in Methods. For the T_{xy} model considered here we find that both $M_{1,2}^{x,y}$ belong to AIII class, while these two matrices are connected by TR symmetry and PH symmetry to recover the symmetries of the original Hamiltonian. In fact the consequence of mirror symmetry for any general Hamiltonian has been intensively studied in literatures[56–59] by defining $\mathcal{M}_{ss'}^\alpha := \mathcal{M}_\alpha \mathbb{T} \mathcal{M}_\alpha^{-1} = s\mathbb{T}, \mathcal{M}_\alpha \mathbb{C} \mathcal{M}_\alpha^{-1} = s'\Sigma$, where $s, s' = \pm 1$. This quantity, $\mathcal{M}_{ss'}^\alpha$, is crucial to determine the possible symmetries of the mirror symmetric invariant subspaces, which are fully consistent with our direct calculations above. This method will be adopted to find *all* the possible mirror symmetric invariant Hamiltonians and their topological classes for all the models presented in Table I.

Topological phases in T_{xy} model. We plot the phase diagram as a function of binding energy ϵ_b and Zeeman field Γ in Fig. 2a, in which the number in each colored regime represents the number of robust Dirac cones. We find that the two fully gapped phases are separated by two gapless phases. The origin of these gapless phases can be understood using the following way. Due to the presence of both PH and TR symmetries, we can define a unitary sublattice symmetry $\mathbb{S} = \mathbb{T} \cdot \mathbb{C}$, which satisfies $\{\mathbb{S}, \mathcal{H}\} = 0$. We then diagonalize this sublattice operator via a unitary transformation $V\mathbb{S}V^{-1} = \mathrm{diag}(\mathbf{I_4}, -\mathbf{I_4})$, under which we have

$$V\mathcal{H}V^\dagger = \begin{pmatrix} 0 & Q \\ Q^\dagger & 0 \end{pmatrix}, \quad \mathrm{Det}\mathcal{H} = |\mathrm{Det}(Q)|^2. \tag{8}$$

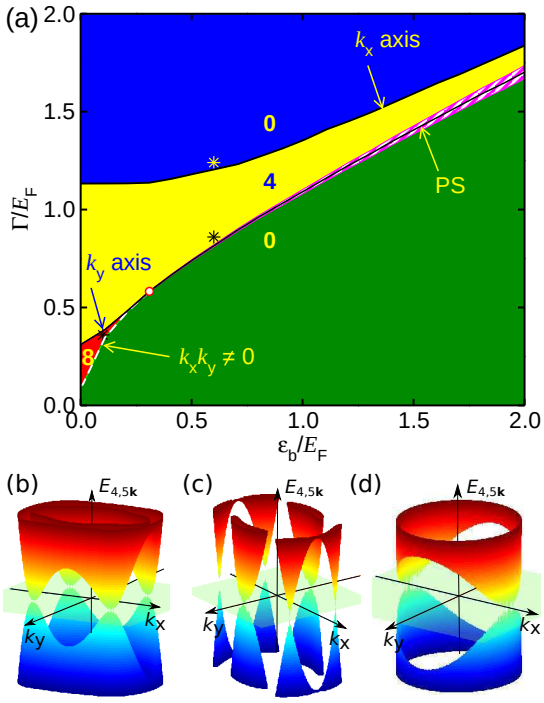

FIG. 2. **Topological superfluids for T_{xy} model**. (a) The phase diagram in the parameter space by ϵ_b and Γ, in which the order parameters and chemical potential are determined self-consistently. The number in each colored regime marks the number of gapless Dirac cones in momentum space, thus 0 defines a fully gapped phase. The two solid line means that the energy gap closing and reopening take place at k_x and k_y axes. The dashed line means gap closing and reopening at nonzero nonzero momenta ($k_x k_y \neq 0$). PS denotes the regime for phase separation, which is visible when $\epsilon_b > 0.3E_F$. Parameters are: $t = 0.6E_F$, $\alpha = 1.0E_F$, $\alpha' = 0.5E_F$. (b) - (d) are band structures at the critical boundaries when $\epsilon_b = 0.1E_F$.

The closing of energy gap means that both the real and imaginary part of $\mathrm{Det}(Q)$ should be zero simultaneously, which give the following two conditions,

$$(\boldsymbol{\gamma} \cdot \mathbf{k})^2 = t^2, \quad \epsilon_{\mathbf{k}}^2 = \Gamma^2 - \Delta^2, \tag{9}$$

where $\boldsymbol{\gamma} = (\alpha', \alpha)$ and $\Delta_1 = \Delta_2 = \Delta$. The first equation defines an ellipse and the second equation defines one circle or two circles, depending strongly on the values of the parameters. The robust gapless phases thus are determined by the overlaps between the ellipse and the circle(s), which may always have intersections in some appropriate parameter regimes. A topological explanation for the robust accidental degeneracy at the Dirac cones and the physical meaning of Eq. 9 will be presented shortly later. When $t \neq 0$, we find the first equation prohibits the gap closing and reopening at zero momentum, thus the topological phase transitions in this model will always take place at nonzero momentum ($\mathbf{k} \neq 0$). This is in sharp contrast to the results in topological D class superconducting phases[12–16, 32, 33] where the critical boundary is only determined by the gap closing and reopening at $\mathbf{k} = 0$.

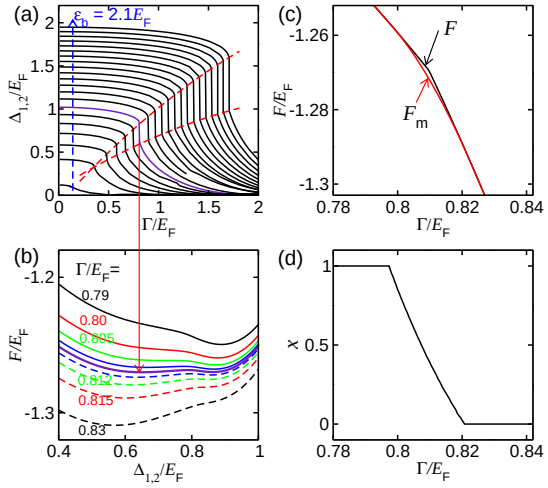

FIG. 3. **Phase separation (PS) in T_{xy} model**. (a) The evolution of order parameters as a function of Zeeman field and binding energy. The regime for sudden jump of order parameters is denoted by the two dashed lines, which happens when $\epsilon_b > 0.3E_F$. (b) The origin of the sudden jump of order parameters from the perspective of free energy F using $\epsilon_b = 0.8E_F$. (c) The mixed free energy F_m (defined in Eq. 18) can have slightly lower energy than F by mixing of two different superfluids. (d) The mixing coefficient x as a function of Zeeman field. For parameters see Fig. 2.

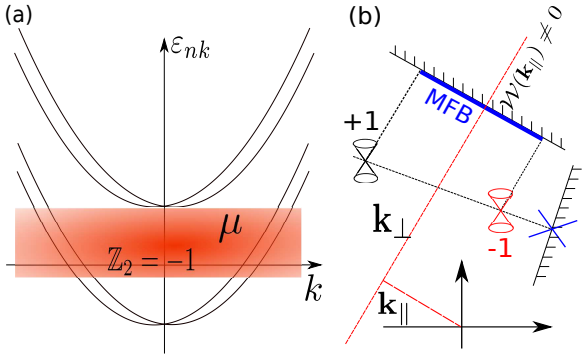

FIG. 4. **Pictures for topological gapped superfluids and MFB.** (a) Topological gapped superfluids with $\mathbb{Z}_2 = -1$ can be realized when the chemical potential μ fills the lowest two bands, thus only one TR invariant point is enclosed by the Fermi surface. This picture holds in the weak pairing limit. (b) The MFB is used to connect the two defects with opposite chiralities (± 1), which can be computed using $\mathcal{W}(\mathbf{k}_\parallel)$ in Eq. 27. The MFB is shrunk to a single point when the line connecting the two defects perpendiculars to the strip direction.

When $t = 0$, the critical boundary is reduced to,

$$\mathbf{k} = 0, \quad \Gamma^2 = \mu^2 + \Delta^2, \tag{10}$$

which is well-known in previous literatures[12–16, 32, 33].

The phase diagram in Fig. 2a can then be understood from how the ellipse intersects with the circle(s). Starting from the fully gapped trivial phase at $\Gamma \sim 0$ and gradually increases the Zeeman fields, we find that the ellipse will first intersect with two circles in the small binding energy regime ($\epsilon_b < 0.3E_F$), in which we observe a topological gapless phase with 8 Dirac cones. This topological phase transition will not take place at the k_x and k_y axes (see Fig. 2b). With the further increasing of Zeeman fields, one of the circles will disappear when $|\mu| < \sqrt{\Gamma^2 - \Delta^2}$ and the system transits to the topological gapless phase with 4 Dirac cones when $\epsilon^2_{\mathbf{k}=(t/\alpha,0)}\epsilon^2_{\mathbf{k}=(0,t/\alpha')} < (\Gamma^2 - \Delta^2)^2$ with gap closing at the k_y axis for the particular parameters used here (see Fig. 2c). Finally, this phase will evolve to the fully gapped phase with gap closing and reopening along the k_x axis (see Fig. 2d). In the large binding energy regime, however, only one circle is allowed in the second equation of Eq. 9 so the fully gapped trivial phase directly enters the phase with 4 Dirac cones. However, this transition will be accompanied by a sudden jump of the order parameter during the topological phase transition, see Fig. 3a. The corresponding jump of the chemical potential is not shown. To understand this effect we calculate the free energy F as a function of order parameters in Fig. 3b, in which two degenerate local minima in F are clearly shown in the critical boundary. The interplay of these two minima gives rise to the jump of parameters in Fig. 3a. The jump of these parameters is an important signal for phase separation (PS)[61, 62]. Fortunately using the method in Refs. [61 and 62] (see Eq. 18 in Methods) we find that the PS phase can only be survived in a narrow regime near the boundary between trivial gapped phase and the gapless phase with 4 Dirac cones.

Next we try to characterize the topology of each phase. We first focus on the fully gapped topological phase at strong Zeeman field, which is characterized by $\mathbb{Z}_2$ from the Cartan classification[17, 18]. We employ the method developed by Qi *et al*[63], $\mathcal{N}_{2d} = \prod_j \mathrm{sgn}(\delta_{j\mathbf{k}})^{p_j}$, where $\delta_{j\mathbf{k}} = \langle j\mathrm{k}|i\mathcal{U}\Delta|j\mathrm{k}\rangle$ is the pairing gap at the jth Fermi surface with $|j\mathbf{k}\rangle$ being the eigenfunction of $\mathcal{H}_0$, and $p_j = 1$ if the TR invariant point at $\mathbf{k} = 0$ is enclosed by the Fermi surface and 0 otherwise. In this formula, $\mathcal{U} = \rho_x \otimes \sigma_y$ and $i\mathcal{U}\bar{\Delta} = \rho_x \otimes \mathbf{I}_2$ is a Hermitian operator thus $\delta_{j\mathbf{k}} \in \mathbb{R}$. Notice that for a relative large pairing strength in this regime, we can always adiabatically deform this state to the weak pairing state near zero binding energy or large Zeeman field without closing the energy gap, thus this criteria can always be applied in this work to characterize the topology of this fully gapped phase. A lengthy but straightforward calculation shows that $\delta_{j\mathbf{k}} = 4\Delta(|t| \pm |\boldsymbol{\gamma}\cdot\mathbf{k}|)/(\Gamma \pm \Upsilon_s)$, where $\pm$ defines the upper and lower two bands and $\Upsilon_s = \sqrt{\Gamma^2 + (|t| + s|\boldsymbol{\gamma}\cdot\mathbf{k}|)^2} \neq 0$. We immediately see from this result that $\delta_{j\mathbf{k}}$ can change sign only when the energy gap is closed at $t \pm |\boldsymbol{\gamma}\cdot\mathbf{k}| = 0$, which is exactly the first equation in Eq. 9. The second equation therefore determines the position of Fermi surface when $\Delta = 0$. Notice that the sign of $\delta_{j\mathbf{k}}$ is fixed in each Fermi surface. Then we find that in this regime, $\mathcal{N}_{2d} = -1$. In this regime the chemical potential just fills the lower two bands while the upper two bands are unoccupied (see Fig. 4a). The same method yields $\mathcal{N}_{2d} = +1$ in the fully gapped trivial phase with small Zeeman field.

This topological gapped phase can support edge states for

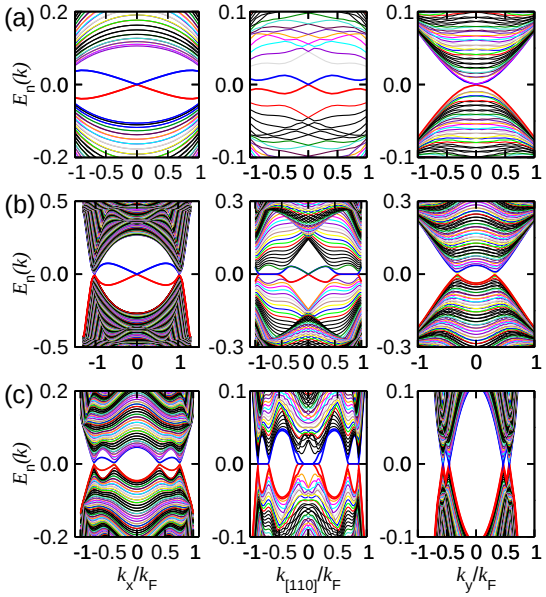

FIG. 5. **Edge states in T_{xy} model along different directions**. Edge states for a strip with $L = 200/k_F$ along k_x (left), $[110]$ (middle) and k_y (right) directions in the fully gapped topological phase (a), gapless phase with 4 (b) and 8 (c) Dirac cones for the three points marked by asterisk (*) in Fig. 2. For parameters see Fig. 2.

a strip along different directions; see Fig. 5a. Note that this gapped phase along k_x and k_y axes may also be protected by mirror symmetry. For this reason, we calculate the topological invariant — the winding number in 1D — in the mirror symmetric invariant subspaces $M^{\alpha}_{1,2}$, which belong to AIII class with only sublattice symmetry. This mirror winding number $\mathcal{W}^{\alpha}$ is calculated using Eq. 27 (see Methods), which are $\mathcal{W}^{x} = 1$ and $\mathcal{W}^{y} = -1$. However, this mirror symmetry can not protect the edge states along other directions.

The topological gapless phases emerged in our model can not be characterized by the previous $\mathbb{Z}_2$ index. Instead, we should use the winding numbers, or equivalently the chiralities, to characterize these topological defects in momentum space. In the vicinity of the defect, the effective Hamiltonian can be written as $H_{\text{eff}} = \sum_{i,j=x,y} v_{ij}(\mathbf{k})\delta k_i \sigma_j$, where $\mathbf{k}$ denotes the position of the defect. The chirality thus is defined as $\nu(\mathbf{k}) = \text{sgn}(\text{Det}[v]) = \pm 1$, where $[v]$ is a matrix constructed by matrix elements v_{ij}. We may also calculate the winding number $\mathcal{W}(\mathbf{k})$ using Eq. 21 for the BdG equation by considering a loop $l : |\mathbf{k} - \mathbf{q}| = r$ around the topological defect. We have a general relation between these two invariants, $\mathcal{W}(\mathbf{k}) = -\nu(\mathbf{k})$ (see Eq. 25 in Methods). The TR symmetry plays a crucial role here because the two topological defects with opposite momenta ($\pm\mathbf{k}$) should have the same chiralities and winding numbers. These defects can only be annihilated by fusing two defects with opposite chiralities. The neutrality of topological charge in the entire space means that some other two topological defects with opposite chiralities should be presented at some other momenta. For this reason, the system can only admit gapless phases with 4 or 8 Dirac cones. It is worth to emphasize that these gapless phases may be a general feature in all topological superconducting phases[26–28].

The edge states in these gapless phases will exhibit some salient anisotropic features along different directions; see Fig. 5b. When the strip is along $[110]$ direction, we observe two MFBs at finite momenta and one in-gap gapless linear excitation near zero momentum. The two MFBs are a typical feature in gapless phases[64], which are used to connect the two Dirac cones with opposite chiralities. These MFBs are protected by topology thus is robust against perturbations. To this end, we can calculate the winding number $\mathcal{W}(\mathbf{k}_{\parallel})$ along an infinity straight line perpendicular the strip direction using Eq. 27 (see Fig. 4b), where $\mathbf{k}_{\parallel}$ is the momentum along the strip direction. We find that $\mathcal{W}(\mathbf{k}_{\parallel}) = -1$, which disappears only when a topological defect is encountered at $\text{Det}Q(\mathbf{k}) = 0$. When the strip is along k_x and k_y directions, the Dirac cones with opposite chiralities are projected to the same points, thus the MFBs are shrunk to some single gapless points.

The second salient feature is about the topological invariant for a fully gapped 1D line in momentum space, which is also characterized by $\mathbb{Z}_2$. The definition of this topological index is identical to that in $\mathcal{N}_{2\text{d}}$[20]. So in the gapless phase regime where the $\mathbb{Z}_2$ index in 2D is ill-defined, we can still define the $\mathbb{Z}_2$ index along some particular directions when the gapless defects are carefully avoided. We find that $\mathcal{N}_{1\text{d}} = -1$ along both k_x and $[110]$ directions, thus for a strip along these directions we can observe some in-gap linear excitations near zero momentum as demonstrated in Fig. 5b. We also find $\mathcal{N}_{1\text{d}} = +1$ when along k_y direction since the gap closing and reopening in the 2D bulk takes place at the k_x axis ($k_y = 0$). As a consequence the in-gap linear excitation near zero momentum is absent. This result is consistent with the mirror winding number analysis which are $\mathcal{W}^{x} = +1$ and $\mathcal{W}^{y} = 0$.

The same analysis can be applied to the regime with 8 Dirac cones, where the major observations are quite similar to the other gapless phase. However, in this regime it is possible to realize $\mathcal{W}(\mathbf{k}_{\parallel}) = 2$ along some particular directions — for instance $[110]$ direction — with doubly degenerate MFBs near zero momentum; see Fig. 5c. Moreover, two MFBs can be found at nonzero momenta. We also found the $\mathbb{Z}_2$ invariant is trivial ($\mathcal{N}_{1\text{d}} = +1$) for a strip along any direction, while in the mirror invariant subspaces we find that the mirror winding number is $\mathcal{W}^{x} = \mathcal{W}^{y} = 0$, so we can not observe any gapless linear excitations near zero momentum in this phase.

While some of these phases are protected by both TR and mirror symmetries, we need to point out that the basic role of mirror symmetry played in this model is quite subtle. In the topological gapped phase we indeed find that the winding number in the mirror invariant subspaces are nonzero. Nevertheless if we artificially break the mirror symmetry by introducing a relative phase to the order parameters, we can still observe these edge states. This means that the TR symmetry is a more important protection in our model. However, in the BDI class phases below, we will show that the mirror symmetry will play the primary role in protecting the edge states in

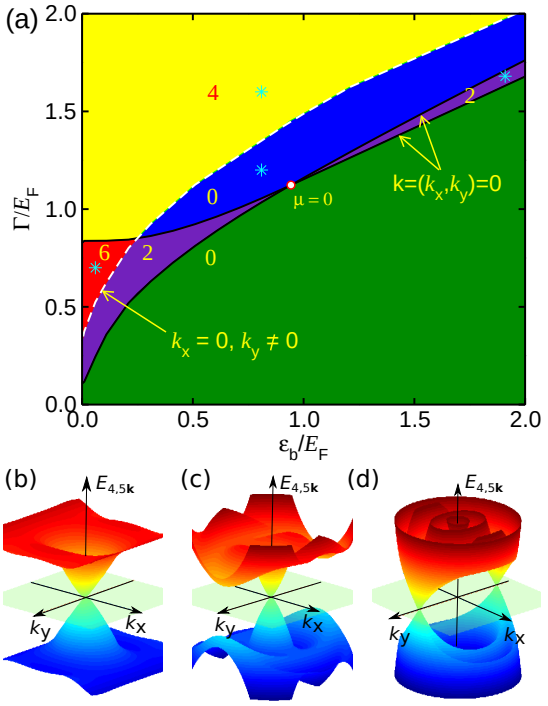

FIG. 6. **Topological superfluids for T_{x0} model**. (a) The phase diagram in the parameter space by $\epsilon_{\rm b}$ and Γ. The meaning of number is the same as that in Fig. 2a. The two solid lines means that the energy gap closing and reopening take place at $\mathbf{k}=0$, and the dashed line means the gap closing and reopening at $k_x=0$ and $k_y\neq 0$. Parameters are: $t_{\uparrow,\downarrow}=0.5E_{\rm F}$, $\alpha=\alpha'=1.0E_{\rm F}$. (b) - (d) show the band structures at the critical boundaries when $\epsilon_{\rm b}=0.5E_{\rm F}$.

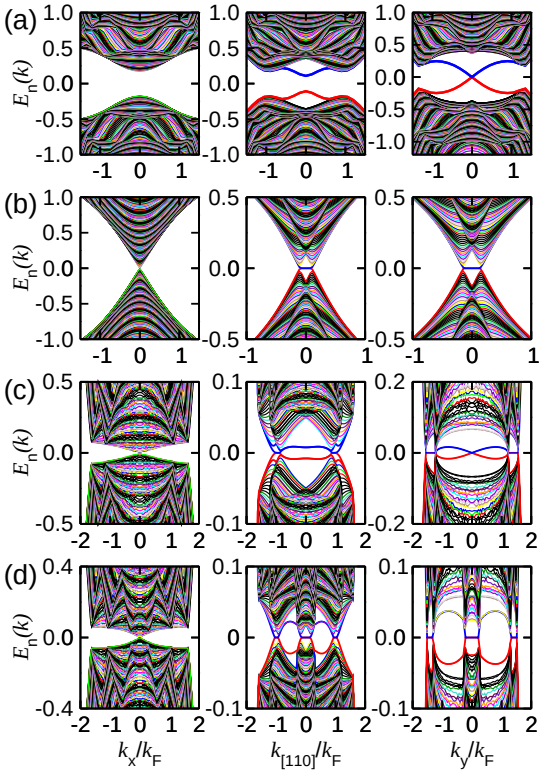

FIG. 7. **Edge states in T_{x0} model along different directions**. Edge states for a strip with width $L=200/k_{\rm F}$ along k_x (left), [110] (middle) and k_y (right) directions in the fully gapped topological phase (a), gapless phase with 2 (b), 4 (c) and 6 (d) Dirac cones for the four points marked by asterisk (*) in Fig. 6. For parameters see Fig. 6.

some parameter regimes.

Topological superfluids with other TR symmetries. Now we try to extend this idea to more general Hamiltonians by assuming that all coefficients — s_i, λ_i, Γ_i and t_σ — can be independently tuned in each layer. In this condition we can perform an exhaustive search strategy to find all possible models with TR symmetry, which belong to either DIII class with $\mathbb{T}^2=-1$ or BDI class with $\mathbb{T}^2=+1$. We first assume that the single particle $\mathcal{H}_0$ has time-reversal symmetry $\mathcal{T}=\mathcal{U}K$, where $\mathcal{U}=\rho_i\otimes\sigma_j$ and $\mathcal{T}\mathcal{H}_0(\mathbf{k})\mathcal{T}^{-1}=\mathcal{H}_0(-\mathbf{k})$. With this operator, we can construct the TR operator for the BdG Hamiltonian, which can be defined as either $\mathbb{T}=\tau_0\otimes\mathcal{U}K$ or $\mathbb{T}=\tau_z\otimes\mathcal{U}K$. For convenience this system is dubbed as T_{ij} model. All the possible results using this method are summarized in Table I, in which only the models with nonzero tunnelings and nonzero SOC coefficients are presented. We find ten different models with TR symmetries, six of which can support nontrivial topological phases. Notice that some of these models require spin-dependent tunnelings, which may be realized by spin selective laser-assisted hopping between the two layers[65] and by modulating the spin-dependent optical lattice[66, 67]. The two layers with different SOC coefficients may need some more complicated laser configurations. There is an interesting relationship between the sign of SOC coefficients and spin-dependent tunnelings, namely, a sign flip for the SOC coefficients s_1/s_2 and λ_1/λ_2 is equivalent to a sign flip in $t_\uparrow/t_\downarrow$, which can be mapped to each other by a unitary transformation. Therefore the T_{xy} and T_{yx}, T_{xx} and T_{yy}, and T_{x0} and T_{xz} are mathematically equivalent, although their physical realizations are totally different. Here we are interested in these models because all these phases may in principle be realized based on s-wave interaction in this versatile platform, where different phases are possible to be tuned to each other.

In all these models, our detailed self-consistent calculation demonstrates that the intimate relation between TR and mirror symmetries is always respected due to the phase locking effect. We determine all the topological classes for the Hamiltonians in the mirror symmetric invariant subspaces using the method in Eq. 7, which are summarized in Table I. The analysis based on the parameter $\mathcal{M}^{\alpha}_{ss'}$ is completely consistent with the direct analysis from the Hamiltonians[56–59]. In all these models the subspaces can belong to AI, AIII and/or BDI classes, where the later two classes can support nontrivial topological phases in 1D[17, 18].

We utilize the T_{x0} model as an example to highlight the unique features of topological superfluids in BDI class. This is also a physical model that may support topological protected MFs in 1D[60]. Unfortunately, this physical model may

TABLE I. **Symmetry table for all the possible superfluids with TR symmetry**. The single particle TR operator is defined as $\mathcal{T} = \mathcal{U}K$, where $\mathcal{U}$ is shown in the second column. The relation between the coefficients Γ_i, s_i, λ_i, t_i and Δ_i are shown from column three to seven, in which the asterisk (*) means that their values can be arbitrary real numbers while $0/0$ means that both the two parameters should be zero simultaneously. $\mathbb{T}$ is the TR operator for the BdG Hamiltonian and $\mathcal{M}^{\alpha}_{ss'}$ defines the symmetry in the mirror invariant subspace. The last column shows whether topological gapped and/or gapless phases can exist (Y) or not (N) in some appropriate parameter regimes.

Model	$\mathcal{U}$	Γ_1/Γ_2	s_1/s_2	λ_1/λ_2	$t_\uparrow/t_\downarrow$	Δ_1/Δ_2	$\mathbb{T}$ ($\mathbb{T}^2$)	Mirror $\mathcal{M}^x_{ss'}$	Mirror $\mathcal{M}^y_{ss'}$	Topo.
T_{xx}	$\rho_x \otimes \sigma_x$	-1	-1	-1	+1	+1	$\tau_z \otimes \mathcal{T}$ (+1)	$\mathcal{M}^x_{+-}$ (AI)	$\mathcal{M}^y_{+-}$ (AI)	N
T_{yy}	$\rho_y \otimes \sigma_y$	-1	+1	+1	-1	-1	$\tau_z \otimes \mathcal{T}$ (+1)	$\mathcal{M}^x_{+-}$ (AI)	$\mathcal{M}^y_{+-}$ (AI)	N
T_{xy}	$\rho_x \otimes \sigma_y$	-1	+1	+1	+1	+1	$\tau_0 \otimes \mathcal{T}$ (-1)	$\mathcal{M}^x_{--}$ (AIII)	$\mathcal{M}^y_{--}$ (AIII)	Y
T_{yx}	$\rho_y \otimes \sigma_x$	-1	-1	-1	-1	-1	$\tau_0 \otimes \mathcal{T}$ (-1)	$\mathcal{M}^x_{--}$ (AIII)	$\mathcal{M}^y_{--}$ (AIII)	Y
T_{xz}	$\rho_x \otimes \sigma_z$	+1	+1	-1	*	-1	$\tau_0 \otimes \mathcal{T}$ (+1)	$\mathcal{M}^x_{+-}$ (AI)	$\mathcal{M}^y_{++}$ (BDI)	Y
T_{x0}	$\rho_x \otimes \sigma_0$	+1	-1	+1	*	+1	$\tau_0 \otimes \mathcal{T}$ (+1)	$\mathcal{M}^x_{+-}$ (AI)	$\mathcal{M}^y_{++}$ (BDI)	Y
T_{zy}	$\rho_z \otimes \sigma_y$	0/0	*	*	-1	*	$\tau_0 \otimes \mathcal{T}$ (-1)	$\mathcal{M}^x_{--}$ (AIII)	$\mathcal{M}^y_{--}$ (AIII)	N
T_{0y}	$\rho_0 \otimes \sigma_y$	0/0	*	*	+1	*	$\tau_0 \otimes \mathcal{T}$ (-1)	$\mathcal{M}^x_{--}$ (AIII)	$\mathcal{M}^y_{--}$ (AIII)	N
T_{0z}	$\rho_0 \otimes \sigma_z$	*	*	0/0	*	*	$\tau_z \otimes \mathcal{T}$ (+1)	—	$\mathcal{M}^y_{+-}$ (AI)	Y
T_{00}	$\rho_0 \otimes \sigma_0$	*	0/0	*	*	*	$\tau_0 \otimes \mathcal{T}$ (+1)	$\mathcal{M}^x_{+-}$ (AI)	—	Y

not have counterpart in solid state systems with 2D SOC, so the realization of topological gapped and gapless superfluids in BDI class is an important extension of our understanding of topological phases. For this model the TR symmetry requires $s_1 = -s_2 = \alpha$, $\lambda_{1,2} = \alpha'$ and $\Gamma_{1,2} = \Gamma$ (see table I). Hereafter we focus on the case $t_{\uparrow,\downarrow} = t$. The phase diagram from the self-consistent calculation is presented in Fig. 6a. To understand the origin of the gapless phases, we calculate the determinant of the Hamiltonian using the method in Eq. 8, which can be written as

$$\mathrm{Det}(Q) = \mathcal{G}(\mathbf{k}) + 8i\alpha' k_x \epsilon_{\mathbf{k}} t\Delta, \tag{11}$$

where $\mathcal{G}(\mathbf{k}) = (\epsilon^2_{\mathbf{k}} - t^2 - k_y^2\alpha^2 - k_x^2\alpha'^2 - \Gamma^2 + \Delta^2)^2 - 4t^2(k_x^2\alpha'^2 + \Gamma^2) + 4(t^2 + k_y^2\alpha^2 + k_x^2\alpha'^2)\Delta^2$, with $\Delta_1 = \Delta_2 = \Delta$. A direct calculation shows that the gapless points can only happen along the k_y axis ($k_x = 0$). Furthermore we can verify easily that when $\Gamma = 0$, $\mathrm{Det}(Q)$ is always greater than zero when $t \neq 0$, so these topological superfluids are also driven by the Zeeman field. In fact we need to emphasize that this is a quite general feature for *all* the topological phases summarized in Table I. Mathematically, the polynominal equation $\mathrm{Det}(Q) = 0$ can always have real solutions in some parameter regimes. In our numerical simulation, we find that the critical boundaries are also determined by three lines as a function of binding energy and Zeeman field. The two solid lines give topological transitions with gap closing and reopening at $\mathbf{k} = 0$ and $(t \pm \mu)^2 + \Delta^2 = \Gamma^2$; see Fig. 6b-c. Obviously these two critical boundaries are reduced to the well-known result in Eq. 10 when $t = 0$. The dashed line is the gap closing and reopening at finite momentum ($k_x = 0, k_y \neq 0$); see Fig. 6d. These critical boundaries are totally different from the T_{xy} model shown in Fig. 2, which can have profound influence on the topological phases with slightly TR symmetry breaking; see below.

We find that in this model the order parameters and chemical potential are always a smooth function of Zeeman field and binding energy, so the PS phase discussed in Fig. 3 is not shown up. However, this model can exhibit some interesting features that not seen in the previous T_{xy} model. We notice that when $\mathbb{T}^2 = +1$ the two Dirac cones with opposite momenta have opposite chiralities (see an exact proof in Methods), so in principle, all the topological protected gapless superfluids with even number (≤ 8) of Dirac cones are admitted. Our crucial observations thus are in order. (**1**) We first focus on the fully gapped phases which in principle can not support topological phases in 2D from the standard table[17, 18]. However, mirror symmetry protected phases are still allowed, which can be characterized by the winding number defined in Eq. 27 along the mirror symmetric invariant subspaces. For the fully gapped phase at small Zeeman field ($\Gamma \sim 0$), we find that the mirror winding numbers along k_y axis are $\mathcal{W}^y_1 \oplus \mathcal{W}^y_2 = 0 \oplus 0$. Notice that the mirror symmetric subspaces along k_x direction belong to AI class thus is always trivial in 1D[17, 18]. For this reason we do not observe gapless excitation for a strip along any directions (not shown in Fig. 7). However, in the fully gapped phase at strong Zeeman field, we find that the mirror winding numbers are $\mathcal{W}^y_1 \oplus \mathcal{W}^y_2 = -1 \oplus -1$ and $\mathcal{W}(\mathbf{k}_\parallel = k_y) = +1$, so we can observe robust gapless excitations for a strip along k_y direction in Fig. 7a. (**2**) In the left phase with 2 Dirac cones, the mirror winding numbers are $\mathcal{W}^y_1 \oplus \mathcal{W}^y_2 = -1 \oplus 0$. thus we observe robust MFBs along both k_y and $[110]$ directions in Fig. 7b. The MFB is shrunk to a single point for a strip along k_x direction since all the Dirac cones are located at the k_y axis. (**3**) In the regime with 4 Dirac cones, the mirror winding numbers are $\mathcal{W}^y_1 \oplus \mathcal{W}^y_2 = -1 \oplus -1$, which are exactly the same as the topological gapped phase at strong Zeeman field due to gap closing and reopening at $k_y \neq 0$. This explains why the similar in-gap excitations in Fig. 7a can also be observed in Fig. 7c. Meanwhile we can observe two MFBs at finite momenta due to the same reason discussed in T_{xy} model. (**4**) In the regime with 6 Dirac cones, the mirror winding numbers are $\mathcal{W}^y_1 \oplus \mathcal{W}^y_2 = -1 \oplus 0$, which are the same as the left gapless phase with 2 Dirac cones in Fig. 7b. In this phase regime we can observe three MFBs for a strip along k_y and $[110]$ directions in Fig. 7d, all of which will shrink to a single point for a

strip along k_x direction. (**5**) These mirror symmetry protected phases will be destroyed by mirror symmetry breaking terms, such as the relative phase between the order parameters.

Discussion and conclusion. Here we investigate the topological phases in ultracold atom systems due to their flexibility of tuning all the parameters in a wide range in experiments, which are challenging in solid state system. In Methods we have shown a concrete scheme to realize the bilayer structure with exactly opposite Zeeman fields. However, it is still very interesting to ask the basic question that what will happen under weak TR symmetry breaking? In this condition both the DIII and BDI class phases will be collapsed to D class phases[32, 33], in which the topological phase transitions can be characterized by either Chern number or Pfaffian aforementioned and all gapless phases will be destroyed. In the T_{xy} model we find that all the phases under weak TR symmetry breaking have Chern number $\mathcal{C} = 0$ and Pfaffian $\chi = \text{sgn Pf}(\mathcal{H}(0)\tau_x) = +1$. This is due to the fact that all the energy gap closings and reopenings in this model take place at nonzero momenta, so the Pfaffian at zero momentum is unchanged. However, the BDI model can exhibit totally different behaviors due to the possibility of gap closing and reopening at zero momentum. So we find that the trivial gapped phase will have $\mathcal{C} = 0$ and $\chi = +1$, and the regime with 2 and 6 Dirac cones will have $\mathcal{C} = 1$ and $\chi = -1$, and the fully gapped topological phase and the regime with 4 Dirac cones will have $\mathcal{C} = 2$ and $\chi = +1$. In general, $\chi = (-1)^{\mathcal{C}}$[69]. If all the parameters in experiments can be changed adiabatically, it is possible to observe the topological transitions among DIII, D and BDI classes without gap closing[68].

We finally emphasize that these phases will not be spoiled by the presence of interlayer pairings. We have included all the interlayer pairings in our model (see Methods) and minimize the total free energy F with respect to these parameters. The detailed self-consistent simulation shows that the TR symmetry is always respected. This is due to the phase locking effect between the two layers with real tunnelings. These pairings only slightly modify the real and imaginary part of Det$Q$ discussed in Eq. 9 and Eq. 11, thus Det$Q = 0$ can always have real solutions in some parameter regimes. Instead, these pairings just slightly modify the topological boundaries without qualitatively influence all the conclusions.

To conclude, the bilayer structure defined in this work provides an experimentally controllable platform to realize new topological protected phases in ultracold atom systems with TR symmetry that belonging to DIII and BDI classes. These phases can be realized using the conventional s-wave interactions, thus is in stark contrast to previous physical proposals based on unconventional pairings. In these models, the fully gapped phase in DIII class is characterized by $\mathbb{Z}_2$, while all the gapless phases in these two classes are characterized by winding numbers around the topological defects. The phase locking effect between the two layers ensures the realization of mirror symmetry protected gapped and gapless phases. These new phases are expected to greatly enrich our understanding of topological superconducting phases and related transitions. This novel idea can also be applied to explore the MFs in 1D and the Weyl superfluids in 3D, and their crossover from the Bose-Einstein condensation in the strong coupling limit to the Bardeen-Cooper-Schrieffer in the weak coupling limit[32–36], which will be published elsewhere.

Methods

Generation of local Zeeman fields in T_{xy} model. The spin-dependent double-well potential in Eq. 3 is essential for the first four models in Table I, which can be realized using the state-of-the-art techniques. Here we follow the basic idea in Ref. [70]. For the cold atom optically pumped from the $|J = 1/2\rangle$ manifold to the $|J' = 3/2\rangle$ manifold and in the large detuning limit the rank 2 polarizability tensor takes the following form[70],

$$\alpha_{ij}(J \to J') = \tilde{\alpha}(\frac{2}{3}\delta_{ij} - \frac{i}{3}\epsilon_{ijk}\sigma_k), \tag{12}$$

where $\tilde{\alpha}$ is a constant that inversely proportional to the detuning. For transparency we first consider two counterpropagating laser beams with momenta $\pm k$ and frequency ω along z direction. Then the electric field can be written as

$$\mathbf{E} = (E_1\mathbf{e}_1 e^{i(kz+\phi)} + E_2\mathbf{e}_2 e^{-ikz})e^{i\omega t}, \tag{13}$$

where $\mathbf{e}_{1,2}$ represent the polarization direction for the two laser beams with field strength $E_{1,2}$, and ϕ is the relative phase between the two laser beams. Let $\mathbf{e}_1 = \cos(\frac{\theta}{2})\mathbf{e}_x + \sin(\frac{\theta}{2})\mathbf{e}_y$ and $\mathbf{e}_2 = \cos(\frac{\theta}{2})\mathbf{e}_x - \sin(\frac{\theta}{2})\mathbf{e}_y$, where θ is the relative polarization angle between the two laser beams, then the spin-dependent optical lattice can be written as[70]

$$U(z) = \mathbf{E}^* \cdot \alpha \cdot \mathbf{E} = \tilde{\alpha}[\frac{2}{3}|\mathbf{E}|^2 + \frac{i}{3}(\mathbf{E}^* \times \mathbf{E}) \cdot \boldsymbol{\sigma}], \tag{14}$$

where in the second term only the σ_z component is nonzero since $\mathbf{E}$ and $\mathbf{E}^*$ lie in the x-y plane. Plugging the expression of $\mathbf{E}$ into Eq. 14 we find

$$U(z) = U[2\cos(\theta)\cos(2kz + \phi) + \sin(\theta)\sin(2kz + \phi)], \tag{15}$$

where $U = -\frac{2}{3}\tilde{\alpha}E_1E_2$. Thus these two laser beams create a spin-dependent periodic optical lattice along z direction.

To realize an isolated double-well structure in Fig. 1a, we can apply two extra laser beams along the same direction with momenta $\pm 2k$[45, 46], polarizability $\tilde{\alpha}'$, electric field strength $E'_{1,2}$ (hence $U' = -\frac{2}{3}\tilde{\alpha}'E'_1E'_2$), polarization angle θ' and relative phase ϕ'. These four colinear laser beams can create a spin-dependent potential in the following form,

$$\begin{aligned} U(z) = {} & 2U\cos(\theta)\cos(2kz) + 2U'\cos(\theta')\cos(4kz + \delta\phi) + \\ & (U\sin(\theta)\sin(2kz) + U'\sin(\theta')\sin(4kz + \delta\phi))\sigma_z, \end{aligned} \tag{16}$$

where a shift of z by $-\phi/2k$ has been made and $\delta\phi = \phi' - 2\phi$. We plot the band structure in Fig. 1b using the above equation with $\delta\phi = 0$, which is exactly the ideal potential presented in Eq. 3. In this potential the first part —an even function of z —gives the symmetric double-well potential while the second part — an odd function of z — gives the spin-dependent

Zeeman fields. The two layers therefore have exactly opposite Zeeman fields and this feature is independent of the choice of other parameters. We also need to emphasize that a bilayer system with TR symmetry can still be achieved even deviates from this idea condition because five independent parameters — U, U', θ, θ', $\delta\phi$ — can be tuned to ensure just two constraints — $t_\uparrow = t_\downarrow$ and $\Gamma_1 = -\Gamma_2$ — in T_{xy} model, which can always be fulfilled in a vast range of parameters. Furthermore the external Zeeman field along z direction, $B_z\sigma_z$, can also contribute to the recovery of TR symmetry.

Self-consistent calculation. The pairings in ultracold atoms is induced by the s-wave scattering between the particles thus should be determined in a self-consistent manner. In the major numerical simulation, we only consider the intralayer pairings by assuming that the interlayer pairings are sufficiently suppressed by the strong barrier between the two layers (see Fig. 1). The thermodynamic potential Ω is defined as $Z = e^{-\Omega/T} = \mathrm{Tr}e^{-H/T}$. When $T \to 0$ we have

$$\Omega = \frac{1}{2}\sum_{\eta<0,\mathbf{k}} (E_{\eta\mathbf{k}} + 2\epsilon_{1\mathbf{k}} + 2\epsilon_{2\mathbf{k}}) + \frac{|\Delta_1|^2}{g} + \frac{|\Delta_2|^2}{g}, \quad (17)$$

where $\eta < 0$ means summation over all the occupied bands with $E_{\eta\mathbf{k}} \leq 0$. The condensation energy should be regularized using the prescription: $g = \sum_{\mathbf{k}} 1/(\mathbf{k}^2/m + \epsilon_{\mathrm{b}})$, where ϵ_{b} defines the binding energy which can be controlled by the Feshbach resonance. The corresponding free energy used in Fig. 3b is defined as $F = \Omega + n\mu$. The order parameters and chemical potential are determined by the extrema of F: $\partial F/\partial\Delta_i = 0$, $\partial F/\partial\Delta_i^* = 0$ and $\partial F/\partial\mu = 0$.

In our simulation, the two order parameters are assumed to $\Delta_1 e^{i\delta\theta}$, and $\Delta_2 e^{-i\delta\theta}$ respectively, where $\Delta_{1,2}$, $\delta\theta \in \mathbb{R}$. The global phase has been gauged out, so $\delta\theta$ determines the relative phase between the order parameters in the two layers. There three parameters together with the chemical potential are used to minimize the total free energy F. In our numerical simulation we have assumed $k_{\mathrm{F}} = \sqrt{n\pi}$, where n is the fixed total particle density, and $E_{\mathrm{F}} = k_{\mathrm{F}}^2/2m$. In all our simulation the energy and momentum are rescaled by E_{F} and k_{F}, respectively. We find that in all our numerical simulation $\delta\theta = 0$, which means that the order parameters between the two layers always have fixed phase. This basic feature, dubbed as phase locking effect throughout this work, is still respected by the presence of interlayer pairings (see below).

Phase separation. The instability of the uniform phases towards the PS phase can be understood from the mixing of two different phases, which is captured by the following mixed free energy[61, 62],

$$F_{\mathrm{m}} = xF(\mu, \Delta_1, \Delta_2) + (1-x)F(\mu, \Delta_1', \Delta_2'), \quad (18)$$

where $0 \leq x \leq 1$ defines the mixing coefficient (see numerical result in Fig. 3d). The two phases should have the same chemical potential but different pairing strengthes $\Delta_{1,2}$ and $\Delta_{1,2}'$. We minimize the total mixed free energy F_{m} with respect to all these parameters to map out the PS phase in Fig. 2a. We find that this phase is not favorable in the T_{x0} model.

Topological invariants in the gapless phases. Now we investigate the effect of TR, PH and mirror symmetries on the winding numbers and chiralities for the gapless phases.

(1) We first notice that the off-diagonal matrix Q in Eq. 8 and Eq. 11 have the following properties[17, 18]

$$\mathrm{Det}[Q_{\mathrm{DIII}}^T(\mathbf{k})] = \mathrm{Det}[-Q_{\mathrm{DIII}}(-\mathbf{k})], \quad \text{and} \quad (19)$$
$$\mathrm{Det}[Q_{\mathrm{BDI}}^*(\mathbf{k})] = \mathrm{Det}[Q_{\mathrm{BDI}}(-\mathbf{k})]. \quad (20)$$

In these models the winding number around a single topological defect is defined as

$$\mathcal{W}(\mathbf{k}) = \frac{i}{4\pi}\oint_l d\mathbf{q}\mathrm{Tr}\mathbb{S}\mathcal{H}^{-1}\partial_{\mathbf{q}}\mathcal{H} = \frac{1}{2\pi}\Im\oint_l d\mathbf{q}\partial_{\mathbf{q}}\mathrm{Det}Q(\mathbf{q}) \in \mathbb{Z}, \quad (21)$$

where $\mathbf{k}$ defines the position of the defect and the loop $l := |\mathbf{q} - \mathbf{k}| = r$ should be small enough to enclose only one defect. We have

$$\mathcal{W}_{\mathrm{DIII}}(\mathbf{k}) = \mathcal{W}_{\mathrm{DIII}}(-\mathbf{k}), \mathcal{W}_{\mathrm{BDI}}(\mathbf{k}) = -\mathcal{W}_{\mathrm{BDI}}(-\mathbf{k}). \quad (22)$$

We see that the TR symmetry plays a fundamental role in deriving the above results. In fact when TR is broken the Q matrix is no longer well-defined and the topological defects are then destroyed. We do not observe the robust Dirac cones in topological D class phases in all our models in Table I by introducing some TR symmetry breaking terms to Eq. 1.

(2) Next we study the chirality of the topological defect. We assume the defect is located at $\mathbf{k}$ with degenerate zero energy eigenvectors $\psi_\pm$, where $\psi_+ = \mathbb{S}\psi_-$ due to chiral symmetry. Based on these functions we can define two chiral basis $\phi_\pm = \psi_+ \pm \psi_-$, which satisfy $\mathbb{S}\phi_\pm = \pm\phi_\pm$. We assume that $H(\mathbf{k} + \delta\mathbf{k}) = H(\mathbf{k}) + M(\delta\mathbf{k})$ in the vicinity of the defect, where $M(\delta\mathbf{k}) = \delta k_x M_x + \delta k_y M_y$. The chiral symmetry ensures that $\mathbb{S}M\mathbb{S}^\dagger = -M$. With these results we readily have $\langle\phi_\pm|M|\phi_\pm\rangle = 0$, and the off-diagonal term, $\langle\phi_+|M|\phi_-\rangle = \langle\psi_+|M|\psi_+\rangle - \langle\psi_-|M|\psi_-\rangle - \langle\psi_+|M|\psi_-\rangle + \langle\psi_-|M|\psi_+\rangle$. Notice that $\langle\psi_+|M|\psi_+\rangle = -\langle\psi_-|M|\psi_-\rangle$ and $\langle\psi_+|M|\psi_-\rangle = -\langle\psi_-|M|\psi_+\rangle$, so the last two terms should be exactly imaginary numbers. Therefore we can assume $\langle\phi_+|M|\phi_-\rangle = a_1\delta k_x + a_2\delta k_y + i(b_1\delta k_x + b_2\delta k_y)$, where $a_{1,2}$, $b_{1,2} \in \mathbb{R}$. The effective Hamiltonian can be written as

$$H_{\mathrm{eff}} = \begin{pmatrix} 0 & c_1\delta k_x + c_2\delta k_y \\ * & 0 \end{pmatrix} = \sum_{ij} v_{ij}\delta k_i\sigma_j, \quad (23)$$

where $c_i = a_i + ib_i$. The effective Hamiltonian constructed in this way can fully embody the importance of TR symmetry in this model. The chirality for Eq. 23 is defined as

$$\nu = \mathrm{sgn}(\mathrm{Det}[v]) = \mathrm{sgn}(b_1a_2 - b_2a_1). \quad (24)$$

We also find a general relation between these invariants,

$$\mathcal{W}(\mathbf{k}) = -\nu(\mathbf{k}). \quad (25)$$

We turn to study the topological charge at $-\mathbf{k}$, which also have two degenerate eigenvectors $\psi_\pm'$ with $\psi_+' = \mathbb{S}\psi_-'$. The

PH and TR symmetries ensure that $\psi'_- = \mathbb{T}\psi_- = \eta\mathbb{C}\psi_+$, and $\psi'_+ = \mathbb{C}\psi_- = \eta\mathbb{T}\psi_+$, where $\eta = \mathbb{T}^2$. The perturbation term is assumed to be M'. Let $\phi'_\pm = \eta\mathbb{T}\psi_+ \pm \mathbb{T}\psi_-$, then

$$\langle\phi'_+|M'|\phi'_-\rangle = \langle\eta\psi_+ - \psi_-|M|\eta\psi_+ + \psi_-\rangle. \quad (26)$$

For DIII model, $\eta = -1$, and $\langle\phi'_+|M'|\phi'_-\rangle = \langle\phi_+|M|\phi_-\rangle$, so the two defects with opposite momenta have the same chirality. They will have opposite chiralities when $\eta = 1$ in BDI model since $\langle\phi'_+|M'|\phi'_-\rangle = (\langle\phi_+|M|\phi_-\rangle)^\dagger$. This analysis is completely consistent with the results in Eqs. 22 and 25.

(3) To understand the origin of the MFBs localized at the boundary of the strip, we consider another integer topological invariant defined as (see Fig. 4b)[31],

$$\mathcal{W}(\mathbf{k}_\parallel) = \frac{1}{2\pi}\Im\int d\mathbf{k}_\perp\partial\mathbf{k}_\perp \ln \mathrm{Det}Q(\mathbf{k}) \in \mathbb{Z}, \quad (27)$$

where $\mathbf{k}_\perp$ is the direction *perpendicular* to the strip. If this number is nonzero, it means topological protected edge states with zero energy can be found at the two boundaries. The number of edge states is defined by $|\mathcal{W}(\mathbf{k}_\parallel)|$.

Mirror symmetries and mirror winding numbers For the T_{xy} model, $M^x_{1,2} = -\epsilon^x_k\sigma_z\otimes\rho_0 - \Gamma\sigma_z\otimes\rho_z - (k_x\alpha' \pm t)\sigma_z\otimes\rho_y - \Delta\sigma_y\otimes\rho_y$, and $M^y_{1,2} = -\epsilon^y_k\sigma_z\otimes\rho_0 - \Gamma\sigma_z\otimes\rho_z + (k_y\alpha \pm t)\sigma_0\otimes\rho_x - \Delta\sigma_y\otimes\rho_y$. Here $\epsilon^{x,y}_k = k^2_{x,y}/2m - \mu$, and ρ and σ are Pauli matrices which do not have the meaning defined in the main text. These two models belong to AIII model with only chiral symmetry and the topological invariant is characterized by $\mathbb{Z}$ in 1D.

For the T_{x0} model only the mirror spaces generated by $\mathcal{M}_y$ is important. For the case studied in the main text, $t_\uparrow = t_\downarrow = t$, $\alpha = \alpha'$ and $M^y_{1,2} = -(\epsilon^y_k \pm t)\sigma_z\otimes\rho_0 + \Gamma\sigma_z\otimes\rho_z - k_x\alpha'\sigma_z\otimes\rho_y - \Delta\sigma_y\otimes\rho_y$. These two Hamiltonians belong to topological BDI class with TR, PH and chiral symmetries, and the invariant is characterized by $\mathbb{Z}$ in 1D.

Since all the above mirror subspaces have chiral symmetry (AIII for T_{xy} and BDI for T_{x0}), we assume s_α is the chiral symmetry operator for M_α (see Eq. 5 and 6), where

$$u_\alpha s_\alpha u^{-1}_\alpha = \begin{pmatrix}\mathbf{I_2} & 0\\ 0 & -\mathbf{I_2}\end{pmatrix}, u_\alpha M^\alpha_i u^{-1}_\alpha = \begin{pmatrix}0 & q^\alpha_i\\ q^{\alpha\dagger}_i & 0\end{pmatrix}. \quad (28)$$

Then the mirror winding number in these mirror symmetric invariant subspaces can be calculated using Eq. 27, in which $\mathcal{H}$ and $\mathbb{S}$ are replaced by M^α_i and s_α. For T_{xy} model, $s_x = \sigma_y\otimes\sigma_z$ and $s_y = \sigma_x\otimes\sigma_0$; and for T_{x0} model $s_y = \sigma_x\otimes\sigma_0$.

There is an important difference between these two models (T_{xy} and T_{x0}) thought the definition of mirror winding numbers is exactly the same. In T_{xy} model, the two mirror subspaces M^α_1 and M^α_2, which belongs to AIII class in both k_x and k_y directions, are not independent, but are related with each other by TR and PH symmetries, thus there is just only one independent winding number $\mathcal{W}^\alpha$ along each direction. In the main text this number is calculated using M^α_1 since $\mathcal{W}^\alpha = \mathcal{W}^\alpha_1 \equiv \mathcal{W}^\alpha_2$. However in T_{x0} model the two mirror symmetric invariant subspaces belong to BDI class when along k_y direction, which have independent TR and PH symmetries, thus the mirror winding numbers are independent. For this reason the mirror topological properties in BDI model are labeled by two integer numbers $\mathcal{W}^y_1\oplus\mathcal{W}^y_2$, where $\mathcal{W}^y_{1,2}$ are calculated for $M^y_{1,2}$ respectively. We do not have to consider the invariant along k_x direction, which is trivial.

Below we summarize the results for mirror winding numbers for all phases in the phase diagrams in the main text. For T_{xy} model, the topological gapped phase has $\mathcal{W}^x_1 = 1$ and $\mathcal{W}^y_1 = -1$; the phase with 4 Dirac cones has $\mathcal{W}^x_1 = 1$ and $\mathcal{W}^y_1 = 0$; and the regime with 8 Dirac cones has $\mathcal{W}^x_1 = 0$ and $\mathcal{W}^y_1 = 0$. For T_{x0} model, the right phase with 2 Dirac cones has $\mathcal{W}^y_1\oplus\mathcal{W}^y_2 = 0\oplus -1$; the left phase with 2 Dirac cones has $\mathcal{W}^y_1\oplus\mathcal{W}^y_2 = -1\oplus 0$; the regime with 4 Dirac cones has $\mathcal{W}^y_1\oplus\mathcal{W}^y_2 = -1\oplus -1$; the regime with 6 Dirac cones has $\mathcal{W}^y_1\oplus\mathcal{W}^y_2 = -1\oplus 0$ and the fully gapped topological phase has $\mathcal{W}^y_1\oplus\mathcal{W}^y_2 = -1\oplus -1$.

Effect of interlayer pairings. For convenience we use the following notations to define all the possible scatterings between the two layers with $g_{\alpha\beta\gamma\delta}$ being the scattering strength and the Greek alphabet being the layer index,

$$F_{\alpha\beta\gamma\delta} := g_{\alpha\beta\gamma\delta}\sum_{\mathbf{k},\mathbf{q}}(c^\dagger_{\alpha\mathbf{k}\uparrow}c^\dagger_{\beta-\mathbf{k}\downarrow})(c_{\gamma\mathbf{q}\downarrow}c_{\delta-\mathbf{q}\uparrow}) \quad (29)$$
$$\simeq \frac{g_{\alpha\beta\gamma\delta}}{g}\cdot[\sum_{\mathbf{k}}\Delta^*_{\alpha\beta}c_{\delta\mathbf{k}\uparrow}c_{\gamma-\mathbf{k}\downarrow} + \mathrm{h.c} + \frac{\Delta^*_{\alpha\beta}\Delta_{\delta\gamma}}{g}].$$

We define the intralayer and interlayer pairings using the following way: $\Delta_{\alpha\beta} = g\langle\sum_{\mathbf{k}}c_{\alpha\mathbf{k}\uparrow}c_{\beta-\mathbf{k}\downarrow}\rangle$, and $\Delta^*_{\alpha\beta} = g\langle\sum_{\mathbf{k}}c_{\beta-\mathbf{k}\downarrow}c_{\alpha\mathbf{k}\uparrow}\rangle$. The leading pairings in the form $\Delta_{\alpha\alpha} = \Delta_\alpha$ have been used in the main text. We have to sum up all possible Feynman diagrams to construct the mean-field BdG equation. To this end, we define $g_{1111} = g_{2222} = g$, $g_{1112} = g_{1121} = \cdots = g'$, and $g_{1122} = g_{1221} = \cdots = g''$, with $g'' < g' \ll g$. Then we can write

$$U = U^\dagger + U^- + U_0, \quad (30)$$

where $U^\dagger = \sum_{\mathbf{k}}\Delta_1 c^\dagger_{1\mathbf{k}\uparrow}c^\dagger_{1-\mathbf{k}\downarrow} + \Delta_2 c^\dagger_{2\mathbf{k}\uparrow}c^\dagger_{2-\mathbf{k}\downarrow} + \Delta_3 c^\dagger_{1\mathbf{k}\uparrow}c^\dagger_{2-\mathbf{k}\downarrow} + \Delta_4 c^\dagger_{2\mathbf{k}\uparrow}c^\dagger_{1-\mathbf{k}\downarrow}$, $U^- = (U^\dagger)^\dagger$, and $U_0 = -\sum_{\alpha,\beta,\gamma,\delta=1,2}\frac{g_{\alpha\beta\gamma\delta}}{g^2}\Delta^*_{\alpha\beta}\Delta_{\delta\gamma}$. Here we have defined four order parameters due to all possible scatterings. In this condition, for the BdG equation in Eq. 1, the off-diagonal block matrix $\bar{\Delta}$ have to be replaced by

$$\bar{\Delta} = \begin{pmatrix}0 & \Delta_1 & 0 & \Delta_3\\ -\Delta_1 & 0 & \Delta_4 & 0\\ 0 & -\Delta_4 & 0 & \Delta_2\\ -\Delta_3 & 0 & -\Delta_2 & 0\end{pmatrix}, \quad (31)$$

where $\Delta_1 = -\Delta_{11} - \frac{g'}{g}(\Delta_{12}+\Delta_{21}) - \frac{g''}{g}\Delta_{22}$, $\Delta_2 = -\Delta_{22} - \frac{g'}{g}(\Delta_{12}+\Delta_{21}) - \frac{g''}{g}\Delta_{11}$, $\Delta_3 = -\frac{g'}{g}(\Delta_{11}+\Delta_{22}) - \frac{g''}{g}(\Delta_{12}+\Delta_{21})$, $\Delta_4 = -\frac{g'}{g}(\Delta_{11}+\Delta_{22}) - \frac{g''}{g}(\Delta_{21}+\Delta_{12})$. The TR symmetry for this new order parameter is still determined by the operator $\mathbb{T}$ used in the main text, but now, $\Delta_{1,2}$ and $\Delta_{3,4}$

should respect some restrict relations. If we define $\mathcal{O} = \Delta_{12} + \Delta_{21}$, then we can simplify the condensation energy

$$-U_0 = \frac{1}{g}(|\Delta_{11}|^2 + |\Delta_{22}|^2) + \frac{g'}{g^2}\mathcal{O}(\Delta_{11} + \Delta_{22} + \Delta_{11}^* + \Delta_{22}^*) + \frac{g''}{g^2}(\mathcal{O}^2 + \Delta_{11}\Delta_{22}^* + \Delta_{11}^*\Delta_{22}). \quad (32)$$

This energy should be used to replace the last two terms in Eq. 17. The self-consistent numerical sumulation demonstrate that all the conclusions obtained in the main text are still valid in the presence of these interlayer pairings.

Acknowledgements We thank Y. X. Zhao, F. Zhang and Z. D. Wang for valuable discussions. C.C., J.L. and M.G. are supported by Hong Kong RGC/GRF Projects (No. 401011, 401113) and The Chinese University of Hong Kong Focused Investments Scheme. B.H. is supported by Natural Science Foundation of Jiangsu Province under Grant No. BK20130424. C.Z. is supported by ARO (W911NF-12-1-0334) AFOSR (FA9550-13-1-0045) and NSF (PHY-1505496).

Author Contributions B.H. and C.C contributes equally to this work. M.G. conceived the idea and supervised the project. B.H. and C.C. performed the self-consistent calculation and symmetry analysis. M.G. and C.Z. wrote this manuscript. All authors participated in discussions about this work. Correspondence and requests for materials should be addressed to M.G. (skylark.gong@gmail.com) and C.Z. (chuanweizhang@utdallas.com).

Competing Interests The authors declare no competing financial interests.

[1] Nayak, C., Simon, S. H., Stern, A., Freedman, M. & Das Sarma, S. Non-Abelian anyons and topological quantum computation. Rev. Mod. Phys. **80**, 1083 (2008).

[2] Matzdorf, R., Fang, Z., Ismail, Zhang, J., Kimura, T., Tokura, Y. Terakura, K., & Plummer, E. W. Ferromagnetism stabilized by lattice distortion at the surface of the p-wave superconductor Sr_2RuO_4. Science, **289**, 746-748 (2000).

[3] Hicks, C. W., Brodsky, D. O., Yelland, E. A., Gibbs, A. S., Bruin, J. A. N., Barber, M. E., Edkins, S. D., Nishimura, K., Yonezawa, S., Maeno, Y., & Mackenzie, A. P. Strong increase of T_c of Sr_2RuO_4 under both tensile and compressive strain. Science, **344**, 283-285 (2014).

[4] Volovik, G. E. The Universe in a Helium Droplet (Oxford Univ. Press, 2003).

[5] Gurarie, V., Radzihovsky, L., & Andreev, A.V. Quantum phase transitions across a p-wave Feshbach resonance. Phys. Rev. Lett. **94**, 230403 (2005).

[6] Levinsen, J., Cooper, N. R., & Shlyapnikov, G. V. Topological $p_x + ip_y$ superfluid phase of fermionic polar molecules, Phys. Rev. A **84**, 013603 (2011).

[7] Read, N., & Green, D. Paired states of fermions in two dimensions with breaking of parity and time-reversal symmetries and the fractional quantum hall effect. Phys. Rev. B **61**, 10267 (2000).

[8] Fu, L., & Kane, C. L. Superconducting proximity effect and Majorana fermions at the surface of a topological insulator. Phys. Rev. Lett. **100**, 096407 (2008).

[9] Lutchyn, R. M., Sau, J. D., & Das Sarma, S. Majorana fermions and a topological phase transition in semiconductor-superconductor heterostructures. Phys. Rev. Lett. **105**, 077001 (2010).

[10] Lutchyn, R. M., Stanescu, T. D., & Das Sarma, S. Search for Majorana fermions in multiband semiconducting nanowires. Phys. Rev. Lett. **106**, 127001 (2011).

[11] Alicea, J., Oreg, Y., Refael, G., Oppen, F. von, & Fisher, M. P. A. Non-Abelian statistics and topological quantum information processing in 1D wire networks. Nat. Phys. **7**, 412 (2011).

[12] Mourik, V., Zuo, K., Frolov, S. M., Plissard, S. R., Bakkers, E. P. A. M., & Kouwenhoven, L. P. Signatures of Majorana fermions in hybrid superconductor-semiconductor nanowire devices. Science **336**, 1003 (2012).

[13] Das, A., Ronen, Y., Most, Y., Oreg, Y., Heiblum, M., & Shtrikman, H. Zero-bias peaks and splitting in an AlInAs nanowire topological superconductor as a signature of Majorana fermions. Nat. Phys. **8**, 887 (2012).

[14] Finck, A. D. K., Harlingen, D. J. V., Mohseni, P. K., Jung, K., & Li, X. Anomalous modulation of a zero-bias peak in a hybrid nanowire-superconductor device. Phys. Rev. Lett. **110**, 126406 (2013).

[15] Deng, M. T., Yu, C. L., Huang, G. Y., Larsson, M., Caroff, P., & Xu, H. Q. Anomalous Zero-Bias Conductance Peak in a NbInSb NanowireNb Hybrid device. Nano. Lett. **12**, 6414 (2012).

[16] Nadj-Perge, S., Drozdov, I. K., Li, J., Chen, H., Jeon, S., Seo, J., MacDonald, A. H., Bernevig, B. A., & Yazdani, A. Observation of Majorana fermions in ferromagnetic atomic chains on a superconductor. Science **346**, 602 (2014).

[17] Schnyder, A. P., Ryu, S., Furusaki, A., & Ludwig, A. W. W. Classification of topological insulators and superconductors in three spatial dimensions. Phys. Rev. B **78**, 195125 (2008).

[18] Kitaev, A. Periodic table for topological insulators and superconductors. AIP Conf. Proc. **1134**, 22-30 (2009).

[19] Kitaev, A. Y. Unpaired Majorana fermions in quantum wires. Phys. Usp. **44**, 131 (2001).

[20] Qi, X., Hughes, T. L., Raghu, S., & Zhang, S. Time-reversal-invariant topological superconductors and superfluids in two and three dimensions. Phys. Rev. Lett. **102**, 187001 (2009).

[21] Fu, L., & Berg, E. Odd-parity topological superconductors: theory and application to $Cu_xBi_2Se_3$. Phys. Rev. Lett. **105**, 097001 (2010).

[22] Sato, M. Topological odd-parity superconductors. Phys. Rev. B **81**, 220504(R) (2010).

[23] Nakosai, S., Budich, J. C., Tanaka, Y., Trauzettel, B., & Nagaosa, N. Majorana bound states and non-local spin correlations in a quantum wire on an unconventional superconductor. Phys. Rev. Lett. **110**, 117002(2013).

[24] Nakosai, S., Tanaka, Y. & Nagaosa, N. Topological superconductivity in bilayer Rashba system. Phys. Rev. Lett. **108**, 147003 (2012).

[25] Wong, C. L. M., & Law, K. T. Majorana Kramers doublets in $d_{x^2-y^2}$-wave superconductors with Rashba spin-orbit coupling. Phys. Rev. B **86**, 184516 (2012).

[26] Zhang, F., Kane, C. L., & Mele, E. J. Time-reversal-invariant topological superconductivity and Majorana Kramers pairs. Phys. Rev. Lett. **111**, 056402(2013).

[27] Zhang, F., Kane, C. L., & Mele, E. J. Topological mirror superconductivity. Phys. Rev. Lett. **111**, 056403 (2013).

[28] Deng, S., Viola, L., & Ortiz, G. Majorana modes in time-reversal invariant s-wave topological superconductors. Phys.

Rev. Lett. **108**, 036803 (2012)
[29] Zhao Y. X., & Wang, Z. D. Topological classification and stability of Fermi surfaces. Phys. Rev. Lett. **110**, 240404 (2013).
[30] Béri, B. Topologically stable gapless phases of time-reversal-invariant superconductors. Phys. Rev. B **81**, 134515 (2010).
[31] Sato, M., Tanaka, Y., Yada, K., & Yokoyama, T. Topology of Andreev bound states with flat dispersion. Phys. Rev. B **83**, 224511 (2011).
[32] Gong, M., Tewari, S., & Zhang, C. BCS-BEC crossover and topological phase transition in 3D spin-orbit coupled degenerate Fermi gases. Phys. Rev. Lett. **107**, 195303 (2011).
[33] Gong, M., Chen, G., Jia, S., & Zhang, C. Searching for Majorana fermions in 2D spin-orbit coupled fermi superfluids at finite temperature. Phys. Rev. Lett. **109**, 105302 (2012).
[34] Hu, H., Jiang, L., Liu, X. J., & Pu, H. Probing anisotropic superfluidity in atomic Fermi gases with Rashba spin-orbit coupling. Phys. Rev. Lett. **107**, 195304 (2011).
[35] Yu, Z. Q. & Zhai, H. Spin-orbit coupled Fermi gases across a Feshbach fesonance. Phys. Rev. Lett. **107**, 195305 (2011).
[36] He, L. & Huang, X. G. BCS-BEC crossover in 2D Fermi gases with Rashba spin-orbit coupling. Phys. Rev. Lett. **108**, 145302 (2012).
[37] Qu, C., Zheng, Z., Gong, M., Xu, Y., Mao, L., Zou, X., Guo, G., & Zhang, C. Topological superfluids with finite-momentum pairing and Majorana fermions,. Nat. Commun. **4**, 2710 (2013).
[38] Zhang, W., & Yi, W. Topological Fulde-Ferrell-Larkin-Ovchinnikov states in spin-orbit-coupled Fermi gases. Nat. Commun. **4**, 2711 (2013).
[39] Cao, Y., Zou, S. H., Liu, X.-J., Yi, S., Long, G. L., & Hu, H. Gapless topological Fulde-Ferrell superfluidity in spin-orbit coupled Fermi gases. Phys. Rev. Lett. **113**, 115302 (2014).
[40] Dong, Y., Dong, L., Gong, M., & Pu, H. Dynamical phases in quenched spin-orbit-coupled degenerate Fermi gas. Nat. Comms. **6**, 6103 (2015).
[41] Radic, J., Natu, S. S., & Galitski, V. Interaction-tuned dynamical transitions in a Rashba spin-orbit-coupled Fermi gas. Phys. Rev. Lett. **112**, 095302 (2014).
[42] Pan, J. S., Liu, X. J., Zhang, W., Yi, W., & Guo, G. C. Topological superradiant states in a degenerate Fermi gas. Phys. Rev. Lett. **115**, 045303 (2015).
[43] Clogston, A. M. Upper limit for the critical field in hard superconductors. Phys. Rev. Lett. **9**, 266 (1962).
[44] Chandrasekhar, B. S. A note on the maximum ciritical field of high-field superconductor. Appl. Phys. Lett. **1**, 7 (1962).
[45] Bloch, I. Ultracold quantum gases in optical lattices. Nat. Phys. **1**, 23-30 (2005).
[46] Cheinet, P., Trotzky, S., Feld, M., Schnorrberger, U., Moreno-Cardoner, M., Fölling, S., & Bloch, I. Counting atoms using interaction blockade in an optical superlattice. Phys. Rev. Lett. **101**, 090404 (2008).
[47] Eisenstein, J. P. & MacDonald, A. H. Bose-Einstein condensation of excitons in bilayer electron systems. Nature **432**, 691 - 694 (2004).
[48] Qiao, Z., Tse, W.-K., Jiang, H., Yao, Y., & Niu, Q. Two-dimensional topological insulator state and topological phase transition in bilayer graphene. Phys. Rev. Lett. **107**, 256801 (2011).
[49] Lin, Y., Jimenez-Garca, K., & Spielman, I. Spin-orbit-coupled Bose-Einstein condensates. Nature **471**, 83 (2011).
[50] Zhang, J., Ji, S., Chen, Z., Zhang, L., Du, Z., Yan, B., Pan, G., Zhao, B., Deng, Y., Zhai, H., Chen, S. & Pan, J. Collective dipole oscillations of a spin-orbit coupled Bose-Einstein condensate. Phys. Rev. Lett. **109**, 115301 (2012).
[51] Wang, P., Yu, Z., Fu, Z., Miao, J., Huang, L., Chai, S., Zhai, H., & Zhang, J. Spin-orbit coupled degenerate Fermi gases. Phys. Rev. Lett. **109**, 095301 (2012).
[52] Cheuk, L., Sommer, A., Hadzibabic, Z., Yefsah, T., Bakr, W., & Zwierlein, M. Raman-induced interactions in a single-component Fermi gas near an s-wave Feshbach resonance. Phys. Rev. Lett. **111**, 095301 (2013).
[53] Qu, C., Hamner, C., Gong, M., Zhang, C., & Engels, P. Observation of Zitterbewegung in a spin-orbit coupled Bose-Einstein condensate. Phys. Rev. A **88**, 021604 (2013).
[54] Hamner, C., Qu, C., Zhang, Y., Chang, J., Gong, M., Zhang, C., & Engels, P. Dicke-type phase transition in a spin-orbit-coupled Bose-Einstein condensate. Nat. Commun. **5**, 4023 (2014).
[55] Huang, L., Meng, Z., Wang, P., Peng, P., Zhang, S., Chen, L., Li, D., Zhou, Q., & Zhang, J. Experimental realization of a two-dimensional synthetic spin-orbit coupling in ultracold Fermi gases. arXiv:1506.02861.
[56] Chiu, C., Yao, H., & Ryu, S. Classification of topological insulators and superconductors in the presence of reflection symmetry. Phys. Rev. B **88**, 075142(2013).
[57] Yao, H., & Ryu, S. Interaction effect on topological classification of superconductors in two dimensions. Phys. Rev. B **88**, 064507 (2013).
[58] Ueno, Y., Yamakage, A., Tanaka, Y., & Sato, M. Symmetry-protected Majorana fermions in topological crystalline superconductors: theory and application to Sr_2RuO_4. Phys. Rev. Lett. **111**, 087002 (2013).
[59] Shiozaki, K., & Sato, M. Topology of crystalline insulators and superconductors. Phys. Rev. B **90**, 165114 (2014) .
[60] Tewari, S., & Sau, J. D. Topological invariants for spin-orbit coupled superconductor nanowires. Phys. Rev. Lett. **109**, 150408 (2012).
[61] Bedaque, P. F., Caldas, H., & Rupak, G. Phase separation in asymmetrical fermion superfluids. Phys. Rev. Lett. **91**, 247002 (2003).
[62] Yi, W., & Guo, G. C. Phase separation in a polarized Fermi gas with spin-orbit coupling. Phys. Rev. A **84**, 031608(R) (2011).
[63] Qi, X., Hughes, T. L., & Zhang, S. Topological invariants for the Fermi surface of a time-reversal-invariant superconductor. Phys. Rev. B **81**, 134508 (2010).
[64] Nakada, K., Fujita, M., Dresselhaus, G., & Dresselhaus, M.S. Edge state in graphene ribbons: nanometer size effect and edge shape dependence. Phys. Rev. B **54**, 17954 (1996).
[65] Miyake, H., Siviloglou, G. A., Kennedy, C. J., Burton, W. C., & Ketterle, W. Realizing the Harper Hamiltonian with laser-assisted tunneling in optical lattices. Phys. Rev. Lett. **111**, 185302 (2013).
[66] Jiménez-García, K., LeBlanc, L. J., Williams, R. A., Beeler, M. C., Qu, C., Gong, M., Zhang, C., & Spielman, I. B. Tunable spin-orbit coupling via strong driving in ultracold-atom systems. Phys. Rev. Lett. **114**, 125301 (2015).
[67] Valle, G. D., Ornigotti, M., Cianci, E., Foglietti, V., Laporta, P., & Longhi, S. Visualization of coherent destruction of tunneling in an optical double well system. Phys. Rev. Lett. **98**, 263601 (2007).
[68] Ezawa, M., Tanaka, Y., Nagaosa, N. Topological phase transition without gap closing. Scientific Reports **3**, 2790 (2013).
[69] Huang, B. B., Chan, C. F., & Gong, M. Large Chern-number topological superfluids in a coupled-layer system. Phys. Rev. B **91**, 134512 (2015).
[70] Deutsch, I. H. & Jessen, P. S. Quantum-state control in optical lattices. Phys. Rev. A **57**, 1972 (1998).